

1 **Distinct CRC-associated Apc mutations dictate response to Tankyrase inhibition.**

2
3
4 Emma M. Schatoff^{ff1,2,3}, Sukanya Goswami¹, Maria Paz Zafra¹, Miguel Foronda¹, Michael Shusterman¹,
5 Benjamin I. Leach¹, Alyna Katti^{1,3}, Bianca J. Diaz^{1,3}, Lukas E. Dow^{1,3,4,*}
6
7

- 8 1. Sandra and Edward Meyer Cancer Center, Department of Medicine, Weill Cornell Medicine, New York,
9 NY
10 2. Weill Cornell / Rockefeller / Sloan Kettering Tri-I MD-PhD program, New York, NY
11 3. Weill Cornell Graduate School of Medical Sciences, Weill Cornell Medicine, New York, NY
12 4. Department of Biochemistry, Weill Cornell Medicine, New York, NY
13
14
15

16 * Correspondence to Lukas Dow: lud2005@med.cornell.edu

17 Mailing address: Belfer Research Building, 413 East 69th Street, BB1318, New York, NY, 10044

18 Phone: +1 646 962 6313
19
20
21

22 **Running title:** Apc truncations determine response to Tankyrase blockade
23

24 **Key words:** APC, CRC, Tankyrase, TNKS, Base editing, CRISPR
25

26 **COI statement**

27 LED is a scientific advisory board member and stockholder in Mirimus Inc., who have licensed shRNA
28 technology that is used in this study. All other authors declare no competing interested.

29 **Abstract**

30 The majority of colorectal cancers (CRCs) show hyperactivated WNT signaling due to inactivating mutations in
31 the APC tumor suppressor. Genetically restoring Apc suppresses WNT and induces rapid and sustained tumor
32 regression, implying that re-engaging this endogenous tumor suppressive mechanism may be an effective
33 therapeutic strategy. Here, using new animal models, human cell lines, and *ex vivo* organoid cultures, we show
34 that Tankyrase (TNKS) inhibition can control WNT hyperactivation and provide long-term tumor control *in*
35 *vivo*, but that effective responses are critically dependent on how APC is disrupted. Mutant APC proteins
36 truncated within the Mutation Cluster Region (MCR) region physically engage the destruction complex and
37 suppress the WNT transcriptional program, while early APC truncations (i.e. *Apc^{Min}*) show limited interaction
38 with AXIN1 and β -catenin, and do not respond to TNKS blockade. Together, this work shows that TNKS
39 inhibition, like APC restoration, can reestablish endogenous control of WNT/ β -catenin signaling, but that APC
40 genotype is a crucial determinant of this response.

41

42

43

44

45 **Statement of Significance**

46 This study reveals how subtle changes to the mutations in a critical colorectal tumor suppressor, APC, influence
47 the cellular response to a targeted therapy. It underscores how investigating the specific genetic alterations that
48 occur in human cancer can identify important biological mechanisms of drug response and resistance.

49 **Introduction**

50 Hyperactivation of the WNT signaling pathway is a hallmark of colorectal cancer (CRC), in most cases (~80%)
51 due to inactivating mutations in the adenomatous polyposis coli (APC) tumor suppressor (1,2). APC is a
52 scaffold protein that coordinates assembly of the destruction complex (DC), made up of core proteins APC,
53 AXIN1, GSK3 β , and CK1 α . The DC regulates WNT signaling via sequential phosphorylation of the WNT
54 master regulator β -catenin, marking it for degradation by the proteasome (3). Previously, using genetically
55 engineered and transplantation-based mouse models, we showed that restoration of endogenous Apc expression
56 drives WNT suppression and rapid regression of CRCs in both the colon and liver (4,5). This work provides *in*
57 *vivo* evidence that re-engaging endogenous regulation of WNT signaling is a potent tumor suppressive strategy.

58 Pharmacologically, it is possible to re-engage DC activity via Tankyrase inhibition (6). Tankyrase 1 and 2
59 (TNKS and TNKS2) are functionally-redundant members of the poly-ADP ribose polymerase (PARP) family.
60 Unlike other PARP proteins, they play no role in DNA repair, but rather potentiate WNT signaling by
61 PARylating AXIN1/2, targeting it for degradation, and decreasing the stability and activity of the DC (7-9).
62 Numerous small molecules that enable selective TNKS1/2 blockade and WNT pathway suppression in CRC cell
63 lines (10-12) and normal mouse intestine (13,14) have been described, yet evidence for suppression of WNT-
64 driven tumor growth *in vivo* is conflicting (15-17). Thus, it is unclear if, and in what context, re-engaging the
65 tumor suppressive DC is an effective approach to control hyperactive WNT/ β -catenin signaling. Given the well-
66 defined and consistent tumor response seen following Apc restoration in shApc mice, we sought to exploit
67 genetically defined *in vivo* and organoid models to determine how TNKS inhibition influences tumor cell
68 behavior after Apc disruption.

69 **Results**

70 We previously showed that the acute response to Apc restoration in intestinal and colonic tumors is cell cycle
71 arrest and differentiation (4,5). To determine whether TNKS1/2 inhibition could elicit a similar response *in vivo*,
72 we established a cohort of tumor-bearing *CAGs-LSL-rtTA3/TRE-GFP-shApc/Lgr5-CreER* (hereafter *TG-shApc*)
73 mice by treatment with 4-hydroxytamoxifen (4OHT; 25mg/kg, single i.p. injection) and doxycycline (dox;
74 200mg/kg in the chow, ad libitum) (Figure 1a, Supplementary Figure 1a). Eight - twelve weeks following tumor
75 initiation, mice were randomized into two treatment arms: TNKS1/2 inhibitor G007-LK (30mg/kg, QD) (16) or
76 vehicle control, for one week. Vehicle-treated mice showed highly proliferative lesions with elevated expression
77 of the stem cell marker *Lgr5*, and limited and sporadic evidence of differentiation markers, Keratin 20 (Krt20)
78 and Intestinal Alkaline Phosphatase (ALPi) (Figure 1b). In contrast, G007-LK-treated and Apc-restored tumors
79 had reduced BrdU incorporation, loss of *Lgr5* expression, and induction of both Krt20 and ALPi (Figure 1b-c).
80 Thus, pharmacological TNKS1/2 inhibition phenocopies the acute, tumor-cell-intrinsic response to genetic
81 restoration of Apc.
82

83 We next sought to confirm our findings in an independent Apc-driven CRC model. *Apc^{Min}* mice carry a
84 heterozygous nonsense mutation at codon 850 of Apc and develop intestinal tumors following spontaneous loss
85 of the wildtype allele (18). We treated tumor-bearing 15-20 week-old *Apc^{Min}* mice for one week with G007-LK
86 (30mg/kg, QD) and measured tumor response on histological cross sections, as described above. Surprisingly,
87 and in contrast to what we observed in the *TG-shApc* model, *Apc^{Min}* tumors were completely insensitive to
88 G007-LK treatment. In fact, while adjacent normal intestine showed elevated Axin1 and decreased Lgr5
89 staining, confirming drug exposure (Supplementary Figure 1b-c), G007-LK-treated tumors maintained
90 proliferation, *Lgr5* expression, and showed minimal Krt20 staining or intestinal Alkaline Phosphatase activity
91 (Figure 1c,d).

92 The difference in tumor response between these two Apc-driven models was striking, and in contrast to a recent
93 report by Tanaka *et. al.*, which suggested that early truncating mutations in APC sensitize cell lines to TNKS
94 inhibition (19). To ensure this conflicting effect was not due to differences in *in vivo* tumor growth kinetics or
95 timing of treatment, we generated *shApc* and *Apc^{Min}* intestinal organoids and treated them *ex vivo* for 3 days with
96 G007-LK (1 μ M). In support of our *in vivo* results, G007-LK-treated *shApc* organoids underwent rapid cell cycle
97 arrest, while *Apc^{Min}* organoids maintained a proliferative phenotype (Figure 1e). RNA expression by quantitative
98 RT-PCR (qPCR) further confirmed that TNKS1/2 inhibition induced Krt20 and reduced Lgr5 in *shApc*
99 organoids, but had no effect in *Apc^{Min}* cultures (Figure 1f). Together, this data supports the notion that TNKS
100 inhibition can effectively promote tumor cell arrest in some contexts.

101 Although BrdU incorporation was significantly decreased in G007-LK-treated *shApc* tumors, the response was
102 less uniform than following genetic Apc restoration (Figure 1b), raising the possibility that variable drug dose
103 or delivery may have impacted tumor response in some cases. Indeed, current TNKS inhibitors show limited
104 oral bioavailability and require daily or twice daily intraperitoneal or intratumoral delivery to achieve effective
105 TNKS blockade (16,20). In addition, in our hands, daily i.p. dosing also produced inflammatory adhesions on
106 the liver spleen and peritoneum, precluding increased or prolonged treatment (Supplementary Figure 1d). To
107 achieve potent, constitutive TNKS blockade without the confounding issue of drug delivery we produced two
108 new transgenic strains (carrying independent tandem shRNAs) that enable dox-inducible silencing of *Tnks1/2*.
109 To do this we first screened a series of *Tnks* and *Tnks2* miRE-based shRNAs using a fluorescent sensor
110 construct and identified the two most potent targeting each gene (Supplementary Figure 2a-c). Importantly, both
111 tandem sh*Tnks1/2* constructs induced Axin1 stabilization comparable to treatment with a small molecule TNKS
112 inhibitor *in vitro* (Supplementary Figure 2d) and *in vivo* (Supplementary Figure 2e).

113 To assess the capacity of *Tnks1/2* blockade to provide long-term tumor control, we crossed each *TG-shTnks1/2*
114 strain to *TG-shApc* mice and treated 6-8 week-old mice with 4-OHT and dox (Figure 2a). In *shApc* mice,
115 numerous GFP+ colon lesions were detectable as early as 4 weeks (Figure 2b), and by 10-12 weeks (endpoint),
116 tumor made up more than a quarter (28%) of the gut (Figure 2c-d). In contrast, *shApc/shTnks* mice showed only
117 individual GFP+ crypts, similar to those seen in *shRenilla* (*shRen*) control mice (Figure 2b-c, Supplementary

118 **Figure 3a**). No adenomas were observed in the colon of *shApc/shTnks* mice up to 150 days (endpoint), at which
119 time most *shApc* mice had become moribund (median survival 111 days) (**Figure 2e**). Similarly, the small
120 intestine of *shApc/shTnks* animals resembled wildtype tissue, with only a few animals displaying small
121 hyperproliferative lesions that made up 0.1-0.5% of the total intestinal area (**Figure 2d**). Tumor suppression was
122 not due to an off-target effect of the Tnks shRNAs, as we observed an identical effect using the second *TG-*
123 *shTnks1/2* strain (**Supplementary Figure 3a-c**). Consistent with the dramatically reduced tumor burden,
124 *shApc/shTnks* mice showed no signs of anemia (reduced hematocrit) that is commonly seen in *shApc* mice with
125 substantial intestinal tumor load (**Figure 2f**).

126 Mirroring what we observed following G007-LK treatment of *Apc^{Min}* mice, genetic Tnks1/2 suppression did not
127 block *Apc^{Min}*-driven tumor growth. Both *Apc^{Min} /shRen* and *Apc^{Min} /shTnks* mice developed highly proliferative
128 colonic and small intestinal tumors with minimal evidence of differentiation (**Figure 2c, Supplementary Figure**
129 **3b**). Accordingly, *Apc^{Min}/shRen* and *Apc^{Min}/shTnks* mice showed no significant difference in relative tumor area,
130 hematocrit, or survival (**Figure 2d-f**).

131 The *in vivo* data described above highlights that response to TNKS inhibition may be dependent on the genetic
132 context of the tumor. We sought to reconcile which model better reflects the biology and therapeutic response of
133 human CRC; therefore, we analyzed two independent clinical datasets (MSK-IMPACT colorectal and TCGA
134 PanCan colorectal cancer) for the type and frequency of APC mutations. Consistent with previous analyses
135 (1,2), APC mutations were present in 1231/1693 (73%) patient samples, with predominantly nonsense mutations
136 throughout the N-terminal half of the gene (**Figure 3a**). Further examination of tumors with two identifiable
137 APC mutations revealed a striking selection for cancers carrying at least one truncating mutation within the
138 mutation cluster region (MCR) that spans amino acids ~1250-1580 (**Figure 3b**). Moreover, cases in which only
139 one allele could be identified showed a further bias toward mutations in the MCR (**Supplementary Figure 4a-b**).
140 These observations are consistent with previous analyses on an independent cohort (21), and strongly implies
141 that accurate genetic models of human CRC should harbor at least one MCR mutation in APC, more C-terminal
142 than either the *Apc^{Min}* or *Apc^{Flox}* alleles (**Figure 3b**).

143 To engineer defined nonsense mutations both preceding and within the MCR, we used recently described
144 optimized base editing tools (22). We transfected wildtype C57Bl/6 intestinal organoids with the FNLS base
145 editing enzyme (22), and sgRNAs targeting codons Q884 (*Apc^{Q884X}*) and Q1405 (*Apc^{Q1405X}*) (**Figure 3c,**
146 **Supplementary Figure 5a-b**). The Q884X mutation closely mimics the R876X allele seen in human CRCs,
147 which truncates APC after the armadillo repeats, but before the first set of 15 amino acid β -catenin binding
148 repeats (**Figure 3c**). Truncation of Apc at Q1405, immediately after the second 20 amino acid repeat (20AAR),
149 removes a conserved 'catenin inhibitory domain' (CID) (**Figure 3c**) that is thought to be critical for proper β -
150 catenin regulation (23,24). Indeed, studies in *Drosophila*, cancer cell lines, and mice have shown this allele
151 promotes high levels of WNT activation (23-26). In addition to engineered *Apc* mutations, we generated *Apc^{Min}*

152 and *shApc* organoids, as well as those with an activating missense mutation in serine 33 of *Ctnnb1* ($\beta\text{cat}^{\text{S33F}}$)
153 (Supplementary Figure 5b); this mutant protein cannot be phosphorylated at S33 by GSK3 β , and is therefore
154 independent of the DC.

155 All mutant organoids could be maintained in the absence of WNT/RSPO ligands, confirming cell intrinsic
156 constitutive activation of WNT signaling. To assess the response to TNKS inhibition, we treated each mutant
157 with G007-LK (1 μM) for 7 days, and quantified cell survival by counting viable organoids. As expected,
158 $\beta\text{cat}^{\text{S33F}}$ showed no change in morphology or viability following G007-LK treatment. Similarly, and consistent
159 with the lack of response in *Apc*^{Min} cells, *Apc*^{Q884X} organoids showed no response to G007-LK. In contrast,
160 *Apc*^{Q1405X} and *shApc* organoids showed reduced crypt branching after 3 days, and were unable to survive 7 days
161 of G007-LK treatment (Figure 3d-e). Importantly, the lack of response to TNKS inhibition in *Apc*^{Q884X} and
162 *Apc*^{Min} cultures was not specific to these similar truncating alleles, as organoids carrying an even earlier
163 truncation, *Apc* ^{Δ 580} (generated from the *Apc*^{fllox} allele (27)), were also resistant to G007-LK treatment
164 (Supplementary Figure 6a). Further, the effect was not specific to G007-LK, as we noted a similar genotype-
165 dependent response with two independent TNKS inhibitors of different chemotypes: NVP656 (20) and XAV939
166 (6)(Supplementary Figure 6b).

167 To gain insight into the molecular events underlying the genotype-dependent response to G007-LK, we
168 performed transcriptome profiling by RNAseq. We treated *wildtype*, *Apc* mutant (*Apc*^{Min}, *Apc*^{Q884X}, *Apc*^{Q1405X},
169 and *shApc*), and *Ctnnb1* mutant ($\beta\text{cat}^{\text{S33F}}$) organoids with 1 μM G007-LK (or DMSO vehicle) for three days and
170 recovered cells for mRNA sequencing. Principle component analysis of the data revealed tight clustering of
171 individual biological replicates of similar genotypes, but broad gene expression differences between organoid
172 groups (Supplementary Figure 7a). More than 80% of the variance in gene expression between groups was
173 accounted for by PC1, which included a number of canonical WNT target genes, including *Sox17*, *Nkd1*, *Wnt6*,
174 and *Prox1*. In general, organoids with $\beta\text{cat}^{\text{S33F}}$ mutations and early *Apc* truncations clustered together and had
175 higher WNT target gene expression, while *Apc*^{Q1405X} and *shApc* organoids had lower WNT target induction,
176 albeit markedly higher than wildtype organoids (Supplementary Figure 7b). Importantly, the transcriptome
177 analysis showed that organoids derived from *Apc*^{Min} mice (*Apc*^{L850X}) and those with a similar base editing-
178 induced mutation (*Apc*^{Q884X}) had highly similar global gene expression patterns (Figure 3f, Supplementary
179 Figure 7a), highlighting the fidelity of base editing for modeling specific genetic alleles in organoids.

180 Treatment with G007-LK did not dramatically alter global gene expression of $\beta\text{cat}^{\text{S33F}}$, *Apc*^{Min}, *Apc*^{Q884X} cultures,
181 but caused a striking shift in the transcriptome of *shApc*, *Apc*^{Q1405X}, and *wildtype* organoids. Indeed, significant
182 gene expression changes (log₂FC >2, adj. p-value <0.01) observed in wildtype cultures following treatment with
183 G007-LK (or RSPO1 withdrawal) were closely mirrored in *shApc* and *Apc*^{Q1405X} organoids (Figure 3f). In
184 contrast, few transcriptional changes were observed in G007-LK-treated *Apc*^{Min} and *Apc*^{Q884X} organoids (28 and
185 56 genes, respectively; log₂FC >2, adj. p-value <0.01), and there were zero (0) significant changes in gene

186 expression observed in $\beta\text{cat}^{\text{S33F}}$ cultures (Table S1). The profound lack of response in $\beta\text{cat}^{\text{S33F}}$ organoids strongly
187 suggests that the primary effect of TNKS inhibition is modulating DC activity via Axin1/2.

188 Gene set enrichment analysis (GSEA) of G007-LK-treated $\text{Apc}^{\text{Q1405X}}$ organoid transcriptomes identified an
189 upregulation of networks related to differentiated intestine function, such as protein and lipid metabolism, and a
190 decrease in cell cycle-related MYC and E2F targets (Figure 3g). Conversely, MYC-related gene sets were
191 actually enriched in G007-LK-treated $\text{Apc}^{\text{Q884X}}$ cells (Supplementary Figure 7c). As expected, G007-LK also
192 induced a significant decrease in WNT/ β catenin signaling in $\text{Apc}^{\text{Q1405X}}$ organoids (Figure 3h, Table S2), while
193 WNT signaling was not significantly altered in $\text{Apc}^{\text{Q884X}}$, Apc^{Min} , or $\beta\text{cat}^{\text{S33F}}$ G007-LK-treated organoids (Figure
194 3h). We next compared our data to two published, experimentally-derived intestinal gene signatures that
195 distinguish crypt-based stem cells and differentiated enterocytes (28,29). In both cases, genes linked with
196 terminal enterocyte differentiation were strongly upregulated following treatment of $\text{Apc}^{\text{Q1405X}}$ organoids with
197 G007-LK, while genes associated with Lgr5-positive stem cells were downregulated (Figure 3i, Supplementary
198 Figure 7d, Supplementary Figure 8). Consistent with transcriptional changes, G007-LK-treated shApc and
199 $\text{Apc}^{\text{Q1405X}}$ organoids showed rapid cell cycle arrest and induction of differentiation markers (Krt20 and Alkaline
200 Phosphatase) (Figure 3j, Supplementary Figure 9a-b). No apparent increase in differentiation or loss of stem cell
201 identity were observed following treatment of $\text{Apc}^{\text{Q884X}}$ or $\beta\text{cat}^{\text{S33F}}$ organoids (Figure 3i-j, Supplementary
202 Figures 7-9). The organoid response to G007-LK was not a transient cell cycle arrest, but likely reflects an
203 enterocyte differentiation program, as organoid survival at 7 days was only slightly improved following washout
204 of the drug after 3 days of treatment (Supplementary Figure 10a-b). Further, the intestinal differentiation
205 response observed in organoids is consistent with what we observed following G007-LK treatment of shApc
206 tumors *in vivo* (Figure 1) or genetic Apc restoration (4). In all, these data support the notion that Tankyrase
207 inhibition re-engages endogenous WNT regulation and normal intestinal differentiation in cells carrying a late
208 APC truncation, closely mimicking the effect Apc restoration (4).

209 To determine whether similar a genotype-dependent response was apparent in human colorectal cancer cells, we
210 used a well-characterized human CRC cell line (DLD1) that carries a late truncating allele of APC (1417X) and
211 shows a marked WNT transcriptional response to TNKS inhibitors. Using Cas9 and an sgRNA analogous to the
212 $\text{Apc}^{\text{Q884X}}$ guide used in the mouse studies (APC^{Q883}), we created multiple independent DLD1 lines with shorter
213 APC truncations (Figure 4a, Supplementary Figure 11a). Consistent with what we observed in mouse
214 organoids, the WNT-suppressive response of G007-LK was abrogated in APC^{Q884} cells (Figure 4b). Similarly,
215 patient-derived human CRC organoids (30) carrying late truncating mutations in APC showed decreased WNT
216 target gene expression (*LGR5* and *AXIN2*) after 3 days of G007-LK treatment (Figure 4c, Supplementary Figure
217 11b-c). Together these data show that TNKS inhibitors can suppresses WNT targets in human colorectal cancer
218 cells carrying MCR APC truncations.

219 Our cellular and transcriptome analyses demonstrate that *Apc*^{Q1405X} organoids show a profound WNT pathway
220 downregulation in response to TNKS1/2 inhibition. Indeed, *Apc*^{Q1405X} organoids showed a marked decrease in
221 non-phosphorylated (active) β -catenin following treatment with G007-LK (Supplementary Figure 12a). To
222 directly test if this was due to increased activity of the DC, we measured physical association of key DC
223 members by immunoprecipitation of Axin1. To produce the cell numbers required for effective
224 immunoprecipitation, we generated 2D cell lines carrying *Kras*^{G12D} and *p53-null* mutations and either *Apc*^{Q884X}
225 or *Apc*^{Q1405X} truncations.

226 Baseline Axin1 levels were higher in *Apc*^{Q884X} cells, but as expected, G007-LK treatment drove Axin1
227 stabilization in both contexts (Supplementary Figure 12b-c). The shorter *Apc*^{Q884X} mutant protein was more
228 abundant than *Apc*^{Q1405X} in intestinal cells; however, Axin1 selectively associated with the longer truncated form
229 (Figure 4d). G007-LK treatment further strengthened this binding and enabled increased association with β -
230 catenin. Consistent with this, G007-LK-treated *Apc*^{Q1405X} cells showed increased phosphorylation of β -catenin at
231 S33/S37/T41 (Figure 4d); We were unable to detect phosphorylated β -catenin in Axin1 IPs, likely due to the
232 rapid release of phospho- β -catenin from this complex. In contrast to *Apc*^{Q1405X}, *Apc*^{Q884X} mutant protein showed
233 no increased binding to Axin1 in the presence of G007-LK, did not enable further β -catenin association, and
234 produced only a minor increase in S33 phosphorylation (Figure 4d).

235 Our organoid data described above indicate that the position of *Apc* truncations dictates response to TNKS1/2
236 inhibition. To directly test this hypothesis *in vivo*, we generated a new *Apc*^{Q1405X} mouse allele by direct base
237 editing in C57Bl/6 zygotes (see Methods for detail). Sanger sequencing of DNA from viable founder mice
238 confirmed the expected C>T transition in 14/30 (47%) animals, with the remaining mice showing a mixture of
239 non-C>T changes, indels, and wildtype sequence (Table S3). As expected, no *Apc*^{Q1405X/Q1405X} founder mice were
240 obtained, due to early embryonic lethality of homozygous *Apc* mutants (31), while *Apc*^{Q1405X} heterozygous mice
241 became moribund by 12-14 weeks of age (median survival: 97 days) (Figure 4e). As commonly observed in
242 other *Apc*-mutant models, early onset anemia correlated with multi-focal adenoma growth throughout the small
243 intestine (most likely following LOH, as occurs in *Apc*^{Min} (18)) (Figure 4f-g).

244 To determine whether established *Apc*^{Q1405X} adenomas were sensitive to TNKS1/2 inhibition, we treated tumor-
245 bearing 10-week-old *Apc*^{Q1405X/+} mice with G007-LK (30mg/kg, QD) or vehicle for 1 week. Histological
246 sections of G007-LK-treated intestinal tumors showed decreased nuclear to cytoplasmic ratio, nuclear
247 polarization, and a transition to differentiated villi-like structures (Figure 4g; H&E). Consistent with this,
248 immunofluorescent staining showed reduced proliferation (Figure 4g-h; BrdU) and induction of differentiation
249 markers (Figure 4g-h; Krt20 and ALPi). In contrast to treated *Apc*^{Min} polyps, *Lgr5* expression was dramatically
250 reduced in *Apc*^{Q1405X} lesions, confirming reduced WNT signaling within the adenoma (Figure 4g; *Lgr5*).
251 Together, this data supports our findings in organoids that truncating mutations in the MCR of APC, render cells
252 sensitive to WNT suppression via TNKS inhibition (Figure 4i).

253 Discussion

254 We previously reported that restoring Apc expression induces sustained tumor regression in CRC (4). Here,
255 using genetically defined animal models, organoids and human cell lines, we show that TNKS inhibition can re-
256 engage the same endogenous tumor suppressive mechanism, but this molecular switch is highly dependent on
257 the specific Apc disruption. Tumor cells containing ‘early’ truncating mutations that eliminate all identified
258 Axin1/2 and β -catenin motifs (e.g. Apc^{Min} , Apc^{Q884X}) do not respond to TNKS inhibition, yet those with an MCR
259 mutation can regulate β -catenin and suppress oncogenic signaling in response to Axin1/2 stabilization. To our
260 knowledge, this is the first *in vivo* demonstration that subtle changes in CRC initiating genetic events can lead to
261 profound changes in response to targeted therapy and has implications for strategies that aim to modulate WNT
262 activity through the DC.

263 Consistent with previously published data (21) we observed in three independent datasets that the majority of
264 CRCs carry at least one nonsense mutation within the MCR (~1250-1580). This mutational pattern is
265 hypothesized to be a selection for mutations that enable oncogenic transformation yet retain partial β -catenin
266 regulation, providing a ‘just right’ level of WNT activation (32-34). Interestingly, APC structure-function
267 studies in CRC cell lines and model organisms suggest that truncations at Q1405 that remove the ‘Catenin
268 inhibitory domain’ (CID) immediately after the second 20AAR, disrupt β -catenin turnover, and thus drive high
269 levels of WNT activation (23,24). Consistent with this, our Apc^{Q1405X} organoids, carrying the same truncating
270 allele, hyperactivate WNT signaling, and heterozygous $Apc^{Q1405X/+}$ mice develop intestinal tumors with 100%
271 penetrance. However, in response to TNKS inhibition, Apc^{Q1405X} can engage the DC to suppress hyperactive
272 WNT signaling; this response would not have been predicted from structure-function models. It is important to
273 note that while most human CRCs harbor both an early and late truncation, and our organoids were engineered
274 to carry two Apc^{Q1405X} alleles, we observed that one of the biological replicates (replicate A) carried an
275 unexpected heterozygous deletion in one allele of Apc ([Supplementary Figure 13a-c](#)). While these cells express
276 only one truncated allele and show moderately higher baseline WNT activity, they have an identical response to
277 TNKS inhibition ([Supplementary Figure 13d](#)), implying that the presence of one MCR truncated allele is
278 sufficient to engage the DC.

279 Given the importance of Apc interaction with β -catenin and the DC, it is somewhat counter-intuitive that shApc
280 organoids and tumors show such robust WNT-suppression and differentiation responses to G007-LK, despite
281 extremely potent knockdown ([Supplementary Figure 14](#)). We propose that the reason underlying the response of
282 shApc cells is the presence of a minimal residual amount of full-length Apc protein that can be detected in
283 complex with Axin1, but not in whole cell lysates ([Supplementary Figure 14](#)). While the amount of Apc is
284 dramatically reduced, the residual protein contains all β -catenin and Axin binding domains that allows it to
285 effectively engage the DC, and following Axin stabilization, drive WNT suppression. The observation that only
286 minimal full-length Apc protein is required for tumor suppression is consistent with our previously published

287 work, which showed that intestinal adenomas have a phenotypic response to genetic Apc restoration even before
288 Apc protein is detectable by western blot (4).

289 In all, these findings highlight that distinct mutations within the same gene can appear phenotypically similar
290 (hyperactive WNT), but have profoundly different biochemical responses to therapies targeting their mechanism
291 of action. This reinforces the need to create accurate and representative genetic models for understanding the
292 molecular events of disease and therapy response.

293 Our results contrast with recent *in vitro* work, which concluded that cells with early APC truncations are
294 uniquely sensitive to TNKS inhibition (19). In our experiments, WNT suppression correlated precisely with cell
295 cycle arrest and differentiation, consistent with the role of WNT as a driver of self-renewal and tumorigenesis.
296 In contrast, while almost all cell lines assessed by Tanaka *et al.* showed WNT suppression following TNKS
297 inhibition, most were not dependent on WNT for survival, and thus classified as resistant (19). We believe it is
298 likely that either the accumulation of specific oncogenic events, or prolonged *in vitro* culture relieved their
299 WNT dependence, confounding the correlation of TNKSi response and APC/WNT alterations. Indeed, one
300 recent study in lung adenocarcinoma demonstrated that WNT/RSPO-dependent 3D organoid cultures become
301 WNT-independent when cultured in 2D (35). Further, Lord and colleagues recently proposed that activating
302 Kras mutations may correlate with resistance to TNKS inhibitors (36). While the latter study did not ascribe a
303 specific mechanism to this possible interaction, it is consistent with multiple observations that concurrent
304 inhibition of classic oncogenic signaling pathways such as MAPK or AKT, enhances the response to TNKS
305 inhibition (12,20,37-39).

306 While TNKS inhibition is unlikely to be used as a monotherapy for cancer treatment, it is perhaps worth
307 (re)considering its utility in patients with Familial Adenomatous Polyposis (FAP), that most commonly carry
308 heterozygous germline mutations in the MCR (40), and ultimately have few options other than surgical removal
309 of the colon. Our data imply that FAP-associated adenomas may respond to TNKS inhibitors, though a number
310 of issues of drug dose, bioavailability, and safety would need to be addressed before they could be considered a
311 viable option.

312 Understanding how specific oncogenic insults drive cell transformation and impact therapy response is a key
313 goal of precision oncology medicine. WNT pathway hyperactivation is a clear cancer driver in a number of
314 malignancies, including CRC (1,4,41,42), and has been suggested as an immune-modulator that may impact
315 response to checkpoint inhibitors (43-45). While WNT-targeted agents have yet to make significant progress in
316 clinical medicine, approaches to block WNT hyperactivation are of keen interest for cancer treatment. Defining
317 the genetic context/s in which they will be effective, as described here, is critical for the future development and
318 application of WNT-targeted therapeutics.

319 **Methods**

320 **Cloning**

321 Individual Tnks and Tnks2 shRNAs were cloned into MLPE vector at XhoI and EcoRI sites as previously
322 described (46). For tandem shRNA cloning, the destination vector containing shRNA #1 was digested with
323 EcoRI for 4 hours at 37°C and incubated with CIP for 30 min at 37°C. shRNA #2 was PCR amplified using
324 miRE-TX_For and miRE_EcoRI_Rev primers (Table S4). Positive clones were identified by restriction digest
325 and validated by Sanger sequencing with mir30_seq primer (Table S4). Tandem shRNA cassettes were shuttled
326 into the col1A1 targeting vector (cTGME) following PCR amplification with miRE_XhoI_For and
327 miRE_EcoRI_Rev primers, and XhoI/EcoRI digest. For the shRNA sensor assay, shRNA target sequences
328 against Tnks and Tnks2 were arrayed, produced as a synthetic gBlock (IDT), and cloned into the 3'UTR of a
329 dTomato sensor vector (XhoI/ EcoRI). For Tnks or Tnks2 specific sensors, gBlocks with only Tnks or Tnks2
330 target sequences were designed and cloned as described above. sgRNA cloning into the vector LRT2B cloning
331 was performed as previously described (22,47). The shApc.2235E retroviral vector used to transduce organoids
332 was generated by Gibson cloning into the pMSCV-rtTA3-miRE vector.

333 **Mutation detection by T7 assay**

334 Cas9-induced mutations were detected using the T7 endonuclease I (NEB). Briefly, the target region
335 surrounding the expected mutation site was PCR-amplified using Herculase II (600675, Agilent Technologies).
336 PCR products were column purified (Qiagen) and subjected to a series of melt-anneal temperature cycles with
337 annealing temperatures gradually lowered in each successive cycle. T7 endonuclease I was then added to
338 selectively digest heteroduplex DNA. Digest products were visualized on a 2.5% agarose gel.

339 **Cells**

340 HEK293T (ATCC CRL-3216) and DLD1 cells (ATCC CCL-221) were purchased from ATCC and maintained
341 in Dulbecco's Modified Eagle's Medium (Corning) supplemented with 10% (v/v) fetal bovine serum (FBS), at
342 37° with 5% CO₂. NIH/3T3 (ATCC CRL-1658) were maintained in Dulbecco's Modified Eagle's Medium
343 (Corning) supplemented with 10% (v/v) bovine calf serum. Cells were regularly tested for mycoplasma using
344 the MycoAlert mycoplasma detection kit (Lonza, #LT07-418) and discarded if found positive.

345 **Virus Production**

346 HEK-293T cells cultured in DMEM + 10%FBS were co-transfected with retroviral vector, CMV-Gag-Pol,
347 CMV-Eco envelope and pcSUPER-shPasha (to prevent miRNA processing of the nascent retroviral RNA
348 transcript). Cells were washed 12-24hrs after transfection and viral supernatants were collected from 36-60hrs
349 post-transfection. Detailed protocol available at: www.dowlab.org/Protocols. For LRT2B-sgRNA virus, no
350 pcSUPER-shPasha was included.

351 **shRNA Sensor Assay**

352 The sensor assay was adapted (48) using NIH-3T3s were cultured in DMEM + 10% Calf Serum. Following
353 transduction, the top 20% brightest dTomato-positive cells were collected by FACS. Sorted cells were
354 subsequently transduced with shRNA virus at 1:10 to achieve approximately single MOI. Five days post
355 infection, dTomato expression was measured by flow cytometry, and knockdown calculated as relative decrease
356 from parental population after subtraction of background signal.

357 **Human Colorectal Cancer Cell Lines and Patient-derived organoid**

358 DLD1 cells were transduced with lentivirus expressing Cas9 (Addgene #110837), in the presence of polybrene
359 (8 μ g/ μ l). Two days after transduction, cells were selected in Puromycin (2 μ g/ml). 1×10^4 DLD-Cas9 cells
360 were plated in a 6 well plate, and transduced with the LRT2B vector (Addgene #110854) containing either
361 hAPC.884 or FANCF.S1 control sgRNAs. Two days after transduction, cells were selected in Blasticidin S
362 (5 μ g/ml). $.3 \times 10^4$ LRT2B-transduced cells were plated for treatment with either DMSO or G007-LK 1 μ M for 3
363 days for RNA and protein collection. Deidentified, patient-derived human colorectal cancer organoids
364 (WCM392 and WCM616; previously described (30)) were obtained from the Institute for Precision Medicine at
365 Weill Cornell Medicine. Organoids were cultured in Basal Media + B27, and treated with either DMSO or
366 G007-LK 1 μ M for 3 days.

367 **ES cell targeting**

368 Embryonic Stem (ES) cells were maintained on irradiated feeders, C57Bl/6 cells were cultured 2i media and
369 KH2 cells were cultured in M15 media, both containing LIF as previously outlined (46). Cells were transfected
370 with targeting vector and *CAGs-FlpE* vector using a Lonza X-unit nucleofactor with P3 buffer kit (Lonza
371 #V4XP-3032). Two days following transfections, cells were treated with media containing 150 μ g/ml
372 hygromycin and individual surviving clones were picked after 9-10 days of selection. Two days after clones
373 were picked hygromycin was removed from the media and cells were cultured in standard M15 thereafter. To
374 confirm single copy integration at the *colla1* locus we first validated expected integration by multiplex *colla1*
375 PCR³, and second, confirmed the presence of a single GFP cassette using the Taqman copy number assay,
376 according to the manufacturer's instructions (Invitrogen).

377 **Isolation and culture of intestinal organoids**

378 Isolation, maintenance and staining of mouse intestinal organoids has been described previously (49,50).
379 Briefly, for isolation, 15 cm of the proximal small intestine was removed and flushed with cold PBS. The
380 intestine was then cut into 5 mm pieces, vigorously resuspended in 5mM EDTA-PBS using a 10ml pipette, and
381 placed at 4°C on a benchtop roller for 10 minutes. This was then repeated for a second time for 30 minutes.
382 After repeated mechanical disruption by pipette, released crypts were mixed with 10ml DMEM Basal Media
383 (Advanced DMEM F/12 containing Pen/Strep, Glutamine, 1mM N-Acetylcysteine (Sigma Aldrich A9165-SG))

384 containing 10 U/ml DNase I (Roche, 04716728001), and filtered sequentially through 100µm and 70µm filters.
385 1ml FBS (final 5%) was added to the filtrate and spun at 1200 RPM for 4 minutes. The purified crypts were
386 resuspended in basal media and mixed 1:10 with Growth Factor Reduced Matrigel (BD, 354230). 40µl of the
387 resuspension was plated per well in a 48 well plate and placed in a 37°C incubator to polymerize for 10 minutes.
388 250µl of small intestinal organoid growth media (Basal Media containing 50 ng/mL EGF (Invitrogen
389 PMG8043), 100ng/ml Noggin (Peprotech 250-38), and 500 ng/mL R-spondin (R&D Systems, 3474-RS-050, or
390 from conditioned media) was then laid on top of the Matrigel. Where indicated, dox was added to experiments at
391 500 ng/ml.

392 For sub-culture and maintenance, media was changed on organoids every two days and they were passaged 1:4
393 every 5-7 days. To passage, the growth media was removed and the Matrigel was resuspended in cold PBS and
394 transferred to a 15ml falcon tube. The organoids were mechanically disassociated using a p1000 or a p200
395 pipette and pipetting 50-100 times. 7 ml of cold PBS was added to the tube and pipetted 20 times to fully wash
396 the cells. The cells were then centrifuged at 1000 RPM for 5 minutes and the supernatant was aspirated. They
397 were then resuspended in GFR Matrigel and replated as above. For freezing, after spinning the cells were
398 resuspended in Basal Media containing 10% FBS and 10% DMSO and stored in liquid nitrogen indefinitely.

399 **Organoid transfection**

400 Murine small intestinal organoids were cultured in transfection medium containing CHIR99021 (5µM) and Y-
401 27632 (10µM) for 2 days prior to transfection. Single cells suspensions were produced by dissociating organoids
402 with TrypLE express (Invitrogen #12604) for 5 min at 37°C. After trypsinization, cell clusters in 300µl
403 transfection medium were combined with 100µl DMEM/F12-Lipofectamine2000 (Invitrogen #11668)-DNA
404 mixture (97ul-2ul-1ug), and transferred into a 48-well culture plate. The plate was centrifuged at 600g at 32°C
405 for 60 min, followed by another 6h incubation at 37°C. The cell clusters were spun down and plated in Matrigel.
406 For selecting organoids with Apc mutants, exogenous R-spondin1 and Noggin were withdrawn 2 days after
407 transfection.

408 **Organoid Drug Treatment and Counts**

409 Organoids were plated in 100 µl Matrigel (2x 50 µl droplets) in one 12 well and cultured in Advanced
410 DMEM/F12 + EGF media with either DMSO or G007-LK 1uM. Three days after plating 8 brightfield images
411 were taken in a vertical line, approximately the length of one droplet. Images were then compiled in one
412 document, and viable organoids were counted for each condition. Organoids were then passaged either 1:2 or
413 1:1 (based on confluency) and then cultured again in DMSO or G007-LK. Day 7 counts were calculated from
414 brightfield images and multiplied by the passaging factor.

415 **EdU Flow Cytometry**

417 Organoid EdU flow cytometry was performed using the Click-iT™ Plus EdU Alexa Fluor™ 647 Flow

418 Cytometry Assay Kit (Thermo Fisher, # C10634). Organoids were first incubated with 10 μ M EdU for 4 hours
419 at 37°C. One well of a 12 well plate was broken up by pipetting vigorously 50 times in 1mL PBS, then diluted in
420 5 mL of PBS. Cells were pelleted at 1100rpm x 4 min at 4°C, then resuspended in 50 μ L TrypLE and incubated
421 at 37°C for 5 mins. 5 mL of PBS was then added to inactivate the TrypLE, and cells were pelleted. Cells were
422 resuspended in 250 μ L of 1% BSA in PBS, transferred to a 1.7 mL tube, and then pelleted at 3000rpm x 4 min.
423 Cells were then resuspended in 100 μ L Click-iT™ fixative, and processed as instructed in the Click-iT™ Plus
424 EdU protocol (starting with Step 4.3). Wash and reaction volumes were 250 μ L.

425 **Animal studies**

426 Production of mice and all treatments described were approved by the Institutional Animal Care and Use
427 Committee (IACUC) at Weill Cornell Medicine (NY), under protocol number 2014-0038. ES cell-derived mice
428 were produced by blastocyst injection and animals were either maintained on a mixed C57B6/129 background
429 for experimental breeding or backcrossed to C57Bl/6N mice. Progeny of both sexes were used for experiments
430 and were genotyped for specific alleles (*Lgr5-GFP-IRES-CreER*, *CAGs-rtTA*, *Col1A1*, *TG-shApc.2235E*, *TG-*
431 *Ren.713*, *TG-shTnks1/2-3341-1328*, *TG-shTnks1/2-1385-3004*, *Apc^{O1405X}*, and *Apc^{Min}*) using primers described in
432 Supplementary Table 3 and protocols available at www.dowlab.org/Protocols. Production of mice and all
433 treatments described were approved by the Institutional Animal Care and Use Committee (IACUC) at Weill
434 Cornell Medicine (NY), under protocol number 2014-0038. For induction of the CreER transgene, animals were
435 administered 4-hydroxytamoxifen (4-OHT; 25mg/kg in 90% v/v corn oil, 10% v/v Ethanol) via i.p. injection.
436 Where required, doxycycline was administered via food pellets (200mg/kg) (Harlan Teklad) from 6-8 weeks of
437 age. For G007-LK treatment studies, G007-LK (30mg/kg, MedChemExpress) was mixed with 20%
438 CremaphorEL and 70% PBS, then delivered by daily i.p. injection. Mice were sacrificed after 7 or 14 days.
439 Animal studies were not blinded during treatment, however, quantitation of tumor burden involved
440 measurements by two parties, one blinded to the treatment groups.

441 **Immunofluorescence and *in situ* hybridization (ISH)**

442 Tissue, fixed in freshly prepared 4% paraformaldehyde for 24 hours, was embedded in paraffin and sectioned by
443 IDEXX RADIL (Columbia, MO). Sections were rehydrated and unmasked (antigen retrieval) by heat treatment
444 for 5 mins in a pressure cooker in 10mM Tris / 1mM EDTA buffer (pH 9) containing 0.05% Tween 20. Sections
445 were blocked in TBS / 0.1% Triton X-100 containing 1% BSA. Organoids were stained as previously described
446 (50), with the following exception: Prior to beginning the EdU/Keratin20 staining, organoids were washed once
447 with 300 μ l PBS, then incubated with 300 μ l Cell Recovery Solution for 20 min on ice. Primary antibodies used
448 were: rabbit anti-KRT20 (1:200, Cell Signaling Technologies, #13063), rat anti-BrdU (1:200, Abcam #ab6326).
449 Secondary antibodies were applied in TBS for 1 hour at room temp in the dark, washed twice with TBS,
450 counterstained for 5 mins with DAPI and mounted in ProLong Gold (Life Technologies, #P36930). Secondary
451 antibodies used were: anti-rabbit 488 (1:500, Abcam, #ab150073) and anti-rat 594 (1:500, Abcam, #ab150156).

452 Intestinal alkaline phosphatase staining was performed using the BCIP/NBT Alkaline Phosphatase (AP)
453 Substrate Kit (Vector Laboratories, # SK-5400) [Note: 1 drop Lemavisole Solution/5mL was added prior to the
454 reaction to inhibit endogenous alkaline phosphatase activity (Vector Labs, # SP-5000)] and counter-stained with
455 Nuclear Fast Red (Sigma-Aldrich, #60700). For Lgr5 ISH, freshly cut 5 micron paraffin sections were stained
456 using RNAscope 2.5 LS Red kit (ACD, cat#322150) and Bond Polymer Refine Red Detection kit (Leica,
457 cat#DS9390) on Leica Bond RX instrument following routine manufacturer protocol ACD 2.5 Red. RNAscope
458 2.5 LS probes for Ms-LGR5 (ACD, cat# 312178). DapB-negative control (ACD, cat#312038) were used with
459 hybridization at 42C for 2 hours. The sections were pre-treated with Leica Bond ER2 Buffer for 20 min at 95C
460 and Protease III (ACD, cat#322102) for 20 min at 40C. After staining the sections were counterstained with
461 Hematoxylin and 10ug/ml DAPI for 10 min and mounted with Mowiol mounting media.

462 **Imaging**

463 Images of fluorescent and IHC stained sections were acquired on a Zeiss Axioscope Imager (chromogenic
464 stains), Nikon Eclipse T1 microscope (IF stains) or Zeiss LSM 880 Laser Scanning Confocal Microscope
465 (organoid stains). Raw .tif files were processed using FIJI (Image J) and/or Photoshop CS (Adobe Systems Inc.,
466 San Jose, CA) to create stacks, adjust levels and/or apply false coloring.

467 **Tumor Quantification**

468 Tumor area in H&E stained slides were quantified using FIJI (Image J). Scanned slides were converted to 8-bit
469 images, one intestinal roll was selected (four rolls per mouse), and an Over/Under threshold was set to capture
470 only cells. The total intestinal area was measured using the 'Measure' feature, and then tumors were then
471 identified, manually traced, and measured. All of the tumor areas were summed, then the ratio of total tumor
472 area: total intestinal area was calculated to determine the Tumor Area for each mouse. Immunofluorescent
473 images of BrdU/DAPI positive tumors were analyzed using FIJI. Images from each channel were exported as
474 separate .tif files, then converted to 16-bit images. The tumor area was traced manually, and the nontumor
475 regions of the image were cleared. A threshold was set to capture only BrdU/DAPI positive cells, then these
476 cells were quantified using the 'Analyze Particles' feature. The ratio of BrdU/DAPI positive cells was then
477 calculated to determine the Fraction of BrdU positive cells within a tumor. IHC images of Alkaline Phosphatase
478 positive tumors were also analyzed using FIJI. Images were converted to 16 bit, and the entire tumor area was
479 traced manually and nontumor regions were cleared from the image. A threshold was then set for the stained
480 areas of the tumor, and the area was quantified using the 'Measure' feature. The total area of the tumor was also
481 measured, and then ratio of Alkaline Phosphatase area: total tumor area was calculated to determine the Fraction
482 of Alkaline Phosphatase Staining.

483 **Protein analysis**

484 Small intestine organoids were grown in 300 μ l of Matrigel in one well of a 6-well dish for 3 days post-passage.
485 Organoids were then recovered from the Matrigel using Cell Recovery Solution(ref). Organoid pellets were

486 lysed in 30 μ l RIPA buffer. Antibodies used for Western blot were: anti-Apc (Millipore, #5535), anti-Axin1
487 (CST, #2087), anti-non-phosphorylated β -catenin (CST, #), anti-phospho- β -catenin S33/S37/T41 (CST, #9561),
488 total β -catenin (CST, #8480), anti-GSK3 (CST, #9832), anti-actin-HRP (Abcam, #ab49900), anti-Tnks1/2
489 (Santa Cruz, # sc-365897), anti-GFP (Abcam, #ab13970), Anti- α -Tubulin (Millipore Sigma, # CP06).

490

491 **Immunoprecipitation**

492 To generate 2D cultures, organoids were broken up by pipetting vigorously 50 times, then diluted in 5 mL of
493 Basal Media. Cells were pelleted at 1100rpm x 4 min at 4°C, then resuspended in 50 μ l TrypLE and incubated at
494 37°C for 5 mins. 5mL of PBS was then added to inactivate the TrypLE, and cells were pelleted. Organoids were
495 resuspended in 2mL Basal Media and plated into one well of a 6 well plate, coated with Rat Tail Collagen I
496 (Thermo Fisher, #A10483-01) at 3 μ g/ml in PBS for 30 min at 37°C. When confluent (approximately 5 days),
497 2D cell lines were passaged with 500 μ l Trypsin, neutralized in 1mL DMEM + 10% FBS, and pelleted. Cells
498 were then resuspended in 2 mL Basal Media and plated on Collagen-coated plates as required. For
499 Immunoprecipitation, cells were then expanded into 2 x 15 cm plates, and when near-confluent, cultured in
500 DMSO or G007-LK (1 μ M) for 24 hours. Cells were washed once with PBS, then scraped into 1mL IP lysis
501 buffer (10mM Tris 7.4, 150mM NaCl, 0.5mM EDTA, 0.5% NP40 + PPI/PI) and centrifuged at 13000rpm x 10
502 min at 4°C. 200 μ l of lysate was used for the immunoprecipitation using 25 μ l Protein-A Dynabeads (Thermo
503 Fisher, #10001D) and incubated with Axin1 (1 μ g, CST, #2087) or IgG (1 μ g, CST, #2729). Beads were washed
504 (200 μ l) and eluted (20 μ l) in IP lysis buffer. 5 μ l 5X SLB was added to the elution, and samples were denatured
505 at 95°C for 5 min.

506

507 **RNA isolation, cDNA synthesis and qPCR**

508 RNA was extracted using TRIzol (Thermo Fisher, #15596018) according to the manufacturer's instructions and
509 contaminating DNA was removed by DNase treatment for 10 mins and column purification (Qiagen RNeasy
510 #74106). cDNA was prepared from 1 μ g total RNA using qScript reverse transcription kit (Quantabio, #95047).
511 Quantitative PCR detection was performed using SYBR green reagents (VWR, #101414-288) and specific
512 primers listed in [Table S4](#).

513

514 **RNA sequencing**

515 Total RNA was isolated using Trizol, DNase treated and purified using the RNeasy mini kit (Qiagen, Hilden,
516 Germany). Following RNA isolation, total RNA integrity was checked using a 2100 Bioanalyzer (Agilent
517 Technologies, Santa Clara, CA). RNA concentrations were measured using the NanoDrop system (Thermo
518 Fisher Scientific, Inc., Waltham, MA). Preparation of RNA sample library and RNA-seq were performed by the
519 Genomics Core Laboratory at Weill Cornell Medicine. Messenger RNA was prepared using TruSeq Stranded
520 mRNA Sample Library Preparation kit (Illumina, San Diego, CA), according to the manufacturer's instructions.

521 The normalized cDNA libraries were pooled and sequenced on Illumina NextSeq500 sequencer with single-end
522 75 cycles.

523 **RNAseq analysis**

524 The quality of raw FASTQ files were checked with FastQC and mapped to mouse reference GRCm38 using
525 STAR two-pass alignment (v2.4.1d; default parameters) (51), and transcript abundance estimates were
526 performed using Kallisto (52), aligned to the same (GRCm38) reference genome. Kallisto transcript count data
527 for each sample was concatenated, and transcript per million (TPM) data was reported for each gene after
528 mapping gene symbols to ensemble IDs using the following R packages (“tximport”, tximportData”,
529 “ensembldb”, and “EnsDb.Mmusculus.v79”). Differential gene expression was estimated using DESeq2 (53).
530 For data visualization and gene ranking, log fold changes were adjusted using the *lfcShrink* command in
531 DESeq2, to minimize the effect size of poorly expressed genes. GSEA analysis (v3.0) was performed on pre-
532 ranked gene sets from differential expression between DMSO and G007-LK-treated groups. We used R (v3.5.1)
533 and R Studio (v1.1.383) to create all visualizations, perform hierarchical clustering and principal component
534 analysis. Volcano plots, heatmaps and other visualizations were produced using the software packages:

535 Enhanced Volcano (<https://bioconductor.org/packages/devel/bioc/html/EnhancedVolcano.html>)

536 Pheatmap (<https://cran.r-project.org/web/packages/pheatmap/index.html>)

537 ggplot2 (<https://cran.r-project.org/web/packages/ggplot2/index.html>)

538 ggsashimi (<https://hub.docker.com/r/guigolab/ggsashimi>) (54)

539

540 **Zygote Injections**

541 mRNA was synthesized with mMACHINE™ T7 ULTRA Transcription Kit (Thermo Fisher,
542 #AM1345). 10 µg of DNA from the CMV-FNLS(RA) vector (Addgene, Plasmid #112671) was linearized with
543 SallI, then DNA was ethanol precipitated, and used for the in vitro transcription reaction. For transgenesis, FNLS
544 mRNA (100ng or 20ng) and 2'-O-methyl 3'phosphorothioate stabilized sgRNA
545 (GTTTCAGAGTGAGCCATGTAG; 100ng/ul; Synthego Corp, CA) were co-delivered by microinjection.
546 Microinjections were performed by the Memorial Sloan Kettering Cancer Center (MSKCC) mouse transgenic
547 core facility, using C57Bl/6J fertilized zygotes. Viable pups were genotyped by PCR and direct Sanger
548 sequencing. Animals were maintained as heterozygotes by breeding to C57Bl/6N mice.

549

550 **Statistical analyses**

551 Statistical tests for all data presented here (other than RNAseq) were performed in GraphPad Prism. Detailed
552 results of each test are provided in [Table S5](#).

553

554 **Data Availability**

555 Raw sequence data is available at the NCBI Sequence Read Archive (SRA) under accession PRJNA524289

556

558 **Acknowledgements**

559 This work was supported by a project grant from the NIH/NCI (CA195787-01) and a Stand Up to Cancer
560 Colorectal Cancer Dream Team Translational Research Grant (SU2C-AACR-DT22-17). Stand Up to Cancer is
561 a division of the Entertainment Industry Foundation. Research grants are administered by the American
562 Association for Cancer Research, the scientific partner of SU2C. We thank Kevin Blighe for assistance with
563 Enhanced Volcano R package. We thank Shiaoqing Gong and the MSKCC Mouse Transgenic Core Facility
564 who performed zygote microinjections, supported in part by a U54 grant from the NIH/NCI (U54OD020355).
565 We thank Katia Manova and Mesruh Turkekel from the Molecular Cytology Core Facility who performed ISH
566 experiments, supported in part by a core grant from the NIH (P30 CA0088748). EMS was supported by a Medical
567 Scientist Training Program grant from the National Institute of General Medical Sciences of the National Institutes
568 of Health under award number T32GM07739 to the Weill Cornell / Rockefeller / Sloan-Kettering Tri-Institutional MD-
569 PhD Program, and an F31 Award from the NCI/NIH under grant number 1 F31 CA224800-01. MPZ is supported in
570 part by National Cancer Institute (NCI) Grant NIH T32 CA203702. LED was supported by a K22 Career
571 Development Award from the NCI/NIH (CA 181280-01). The content is solely the responsibility of the authors and
572 does not necessarily represent the official views of the NIH.

573

574 **Author Contributions**

575 EMS designed and performed experiments, analyzed data and wrote the paper. SG, MPZ, AK, MS, BIL, MF,
576 and BJD performed experiments and analyzed data. LED designed and supervised experiments, analyzed data,
577 and wrote the paper.

578

579 **References**

580

- 581 1. Cancer Genome Atlas N. Comprehensive molecular characterization of human colon and rectal cancer.
582 Nature **2012**;487(7407):330-7 doi 10.1038/nature11252.
- 583 2. Zehir A, Benayed R, Shah RH, Syed A, Middha S, Kim HR, *et al.* Mutational landscape of metastatic
584 cancer revealed from prospective clinical sequencing of 10,000 patients. Nat Med **2017**;23(6):703-13
585 doi 10.1038/nm.4333.
- 586 3. Stamos JL, Weis WI. The beta-catenin destruction complex. Cold Spring Harb Perspect Biol
587 **2013**;5(1):a007898 doi 10.1101/cshperspect.a007898.
- 588 4. Dow LE, O'Rourke KP, Simon J, Tschaharganeh DF, van Es JH, Clevers H, *et al.* Apc Restoration
589 Promotes Cellular Differentiation and Reestablishes Crypt Homeostasis in Colorectal Cancer. Cell
590 **2015**;161(7):1539-52 doi 10.1016/j.cell.2015.05.033.
- 591 5. O'Rourke KP, Loizou E, Livshits G, Schatoff EM, Baslan T, Machado E, *et al.* Transplantation of
592 engineered organoids enables rapid generation of metastatic mouse models of colorectal cancer. Nat
593 Biotechnol **2017**;35(6):577-82 doi 10.1038/nbt.3837.
- 594 6. Huang SM, Mishina YM, Liu S, Cheung A, Stegmeier F, Michaud GA, *et al.* Tankyrase inhibition
595 stabilizes axin and antagonizes Wnt signalling. Nature **2009**;461(7264):614-20 doi
596 10.1038/nature08356.
- 597 7. Riffell JL, Lord CJ, Ashworth A. Tankyrase-targeted therapeutics: expanding opportunities in the PARP
598 family. Nature reviews **2012**;11(12):923-36 doi 10.1038/nrd3868.
- 599 8. Lehtio L, Chi NW, Krauss S. Tankyrases as drug targets. Febs J **2013**;280(15):3576-93 doi
600 10.1111/febs.12320.
- 601 9. Haikarainen T, Krauss S, Lehtio L. Tankyrases: structure, function and therapeutic implications in
602 cancer. Curr Pharm Des **2014**;20(41):6472-88.
- 603 10. Chen B, Dodge ME, Tang W, Lu J, Ma Z, Fan CW, *et al.* Small molecule-mediated disruption of Wnt-
604 dependent signaling in tissue regeneration and cancer. Nat Chem Biol **2009**;5(2):100-7 doi
605 10.1038/nchembio.137.
- 606 11. Bao R, Christova T, Song S, Angers S, Yan X, Attisano L. Inhibition of tankyrases induces Axin
607 stabilization and blocks Wnt signalling in breast cancer cells. PLoS ONE **2012**;7(11):e48670 doi
608 10.1371/journal.pone.0048670.
- 609 12. Schoumacher M, Hurov KE, Lehar J, Yan-Neale Y, Mishina Y, Sonkin D, *et al.* Inhibiting Tankyrases
610 sensitizes KRAS-mutant cancer cells to MEK inhibitors via FGFR2 feedback signaling. Cancer Res
611 **2014**;74(12):3294-305 doi 10.1158/0008-5472.CAN-14-0138-T.
- 612 13. Norum JH, Skarpen E, Brech A, Kuiper R, Waaler J, Krauss S, *et al.* The tankyrase inhibitor G007-LK
613 inhibits small intestine LGR5(+) stem cell proliferation without altering tissue morphology. Biol Res
614 **2018**;51(1):3 doi 10.1186/s40659-017-0151-6.
- 615 14. Ye P, Chiang YJ, Qi Z, Li Y, Wang S, Liu Y, *et al.* Tankyrases maintain homeostasis of intestinal
616 epithelium by preventing cell death. PLoS Genet **2018**;14(9):e1007697 doi
617 10.1371/journal.pgen.1007697.
- 618 15. Zhong Y, Katavolos P, Nguyen T, Lau T, Boggs J, Sambrone A, *et al.* Tankyrase Inhibition Causes
619 Reversible Intestinal Toxicity in Mice with a Therapeutic Index < 1. Toxicol Pathol **2016**;44(2):267-78
620 doi 10.1177/0192623315621192.
- 621 16. Lau T, Chan E, Callow M, Waaler J, Boggs J, Blake RA, *et al.* A novel tankyrase small-molecule
622 inhibitor suppresses APC mutation-driven colorectal tumor growth. Cancer Res **2013**;73(10):3132-44
623 doi 10.1158/0008-5472.CAN-12-4562.
- 624 17. Waaler J, Machon O, Tumova L, Dinh H, Korinek V, Wilson SR, *et al.* A novel tankyrase inhibitor
625 decreases canonical Wnt signaling in colon carcinoma cells and reduces tumor growth in conditional
626 APC mutant mice. Cancer Res **2012**;72(11):2822-32 doi 10.1158/0008-5472.CAN-11-3336.
- 627 18. Levy DB, Smith KJ, Beazer-Barclay Y, Hamilton SR, Vogelstein B, Kinzler KW. Inactivation of both
628 APC alleles in human and mouse tumors. Cancer Res **1994**;54(22):5953-8.

- 629 19. Tanaka N, Mashima T, Mizutani A, Sato A, Aoyama A, Gong B, *et al.* APC Mutations as a Potential
630 Biomarker for Sensitivity to Tankyrase Inhibitors in Colorectal Cancer. *Mol Cancer Ther*
631 **2017**;16(4):752-62 doi 10.1158/1535-7163.MCT-16-0578.
- 632 20. Arques O, Chicote I, Puig I, Tenbaum SP, Argiles G, Dienstmann R, *et al.* Tankyrase Inhibition Blocks
633 Wnt/beta-Catenin Pathway and Reverts Resistance to PI3K and AKT Inhibitors in the Treatment of
634 Colorectal Cancer. *Clin Cancer Res* **2016**;22(3):644-56 doi 10.1158/1078-0432.CCR-14-3081.
- 635 21. Christie M, Jorissen RN, Mouradov D, Sakthianandeswaren A, Li S, Day F, *et al.* Different APC
636 genotypes in proximal and distal sporadic colorectal cancers suggest distinct WNT/beta-catenin
637 signalling thresholds for tumorigenesis. *Oncogene* **2013**;32(39):4675-82 doi 10.1038/onc.2012.486.
- 638 22. Zafra MP, Schatoff EM, Katti A, Foronda M, Breinig M, Schweitzer AY, *et al.* Optimized base editors
639 enable efficient editing in cells, organoids and mice. *Nat Biotechnol* **2018**;36(9):888-93 doi
640 10.1038/nbt.4194.
- 641 23. Kohler EM, Chandra SH, Behrens J, Schneikert J. Beta-catenin degradation mediated by the CID
642 domain of APC provides a model for the selection of APC mutations in colorectal, desmoid and
643 duodenal tumours. *Hum Mol Genet* **2009**;18(2):213-26 doi 10.1093/hmg/ddn338.
- 644 24. Roberts DM, Pronobis MI, Poulton JS, Waldmann JD, Stephenson EM, Hanna S, *et al.* Deconstructing
645 the sscatenin destruction complex: mechanistic roles for the tumor suppressor APC in regulating Wnt
646 signaling. *Molecular biology of the cell* **2011** doi 10.1091/mbc.E10-11-0871.
- 647 25. Kohler EM, Derungs A, Daum G, Behrens J, Schneikert J. Functional definition of the mutation cluster
648 region of adenomatous polyposis coli in colorectal tumours. *Hum Mol Genet* **2008**;17(13):1978-87 doi
649 10.1093/hmg/ddn095.
- 650 26. Zeineldin M, Neufeld KL. Understanding phenotypic variation in rodent models with germline *Apc*
651 mutations. *Cancer Res* **2013**;73(8):2389-99 doi 10.1158/0008-5472.CAN-12-4607.
- 652 27. Kuraguchi M, Wang X-P, Bronson RT, Rothenberg R, Ohene-Baah NY, Lund JJ, *et al.* Adenomatous
653 polyposis coli (APC) is required for normal development of skin and thymus. *PLoS genetics*
654 **2006**;2(9):e146 doi 10.1371/journal.pgen.0020146.
- 655 28. Kim TH, Li F, Ferreira-Neira I, Ho LL, Luyten A, Nalapareddy K, *et al.* Broadly permissive intestinal
656 chromatin underlies lateral inhibition and cell plasticity. *Nature* **2014**;506(7489):511-5 doi
657 10.1038/nature12903.
- 658 29. Moor AE, Harnik Y, Ben-Moshe S, Massasa EE, Rozenberg M, Eilam R, *et al.* Spatial Reconstruction
659 of Single Enterocytes Uncovers Broad Zonation along the Intestinal Villus Axis. *Cell*
660 **2018**;175(4):1156-67 e15 doi 10.1016/j.cell.2018.08.063.
- 661 30. Pauli C, Hopkins BD, Prandi D, Shaw R, Fedrizzi T, Sboner A, *et al.* Personalized In Vitro and In Vivo
662 Cancer Models to Guide Precision Medicine. *Cancer Discov* **2017**;7(5):462-77 doi 10.1158/2159-
663 8290.CD-16-1154.
- 664 31. Moser AR, Shoemaker AR, Connelly CS, Clipson L, Gould KA, Luongo C, *et al.* Homozygosity for the
665 *Min* allele of *Apc* results in disruption of mouse development prior to gastrulation. *Dev Dyn*
666 **1995**;203(4):422-33.
- 667 32. Albuquerque C, Breukel C, van der Luijt R, Fidalgo P, Lage P, Slors FJ, *et al.* The 'just-right' signaling
668 model: APC somatic mutations are selected based on a specific level of activation of the beta-catenin
669 signaling cascade. *Hum Mol Genet* **2002**;11(13):1549-60.
- 670 33. Lamlum H, Ilyas M, Rowan A, Clark S, Johnson V, Bell J, *et al.* The type of somatic mutation at APC
671 in familial adenomatous polyposis is determined by the site of the germline mutation: a new facet to
672 Knudson's 'two-hit' hypothesis. *Nat Med* **1999**;5(9):1071-5 doi 10.1038/12511.
- 673 34. Crabtree M, Sieber OM, Lipton L, Hodgson SV, Lamlum H, Thomas HJ, *et al.* Refining the relation
674 between 'first hits' and 'second hits' at the APC locus: the 'loose fit' model and evidence for differences
675 in somatic mutation spectra among patients. *Oncogene* **2003**;22(27):4257-65 doi
676 10.1038/sj.onc.1206471.
- 677 35. Guimaraes PPG, Tan M, Tammela T, Wu K, Chung A, Oberli M, *et al.* Potent in vivo lung cancer Wnt
678 signaling inhibition via cyclodextrin-LGK974 inclusion complexes. *J Control Release* **2018**;290:75-87
679 doi 10.1016/j.jconrel.2018.09.025.

- 680 36. Menon M, Elliott R, Bowers L, Balan N, Rafiq R, Costa-Cabral S, *et al.* A novel tankyrase inhibitor,
681 MSC2504877, enhances the effects of clinical CDK4/6 inhibitors. *Sci Rep* **2019**;9(1):201 doi
682 10.1038/s41598-018-36447-4.
- 683 37. Wang H, Lu B, Castillo J, Zhang Y, Yang Z, McAllister G, *et al.* Tankyrase Inhibitor Sensitizes Lung
684 Cancer Cells to Endothelial Growth Factor Receptor (EGFR) Inhibition via Stabilizing Angiomotins and
685 Inhibiting YAP Signaling. *J Biol Chem* **2016**;291(29):15256-66 doi 10.1074/jbc.M116.722967.
- 686 38. Wu X, Luo F, Li J, Zhong X, Liu K. Tankyrase 1 inhibitor XAV939 increases chemosensitivity in
687 colon cancer cell lines via inhibition of the Wnt signaling pathway. *Int J Oncol* **2016**;48(4):1333-40 doi
688 10.3892/ijo.2016.3360.
- 689 39. Solberg NT, Waaler J, Lund K, Mygland L, Olsen PA, Krauss S. TANKYRASE Inhibition Enhances
690 the Antiproliferative Effect of PI3K and EGFR Inhibition, Mutually Affecting beta-CATENIN and
691 AKT Signaling in Colorectal Cancer. *Mol Cancer Res* **2018**;16(3):543-53 doi 10.1158/1541-
692 7786.MCR-17-0362.
- 693 40. Nieuwenhuis MH, Vasen HF. Correlations between mutation site in APC and phenotype of familial
694 adenomatous polyposis (FAP): a review of the literature. *Crit Rev Oncol Hematol* **2007**;61(2):153-61
695 doi 10.1016/j.critrevonc.2006.07.004.
- 696 41. Nusse R, Clevers H. Wnt/beta-Catenin Signaling, Disease, and Emerging Therapeutic Modalities. *Cell*
697 **2017**;169(6):985-99 doi 10.1016/j.cell.2017.05.016.
- 698 42. Kahn M. Can we safely target the WNT pathway? *Nature reviews* **2014**;13(7):513-32 doi
699 10.1038/nrd4233.
- 700 43. Luke JJ, Bao R, Sweis RF, Spranger S, Gajewski TF. WNT/beta-catenin Pathway Activation Correlates
701 with Immune Exclusion across Human Cancers. *Clin Cancer Res* **2019**;25(10):3074-83 doi
702 10.1158/1078-0432.CCR-18-1942.
- 703 44. Grasso CS, Giannakis M, Wells DK, Hamada T, Mu XJ, Quist M, *et al.* Genetic Mechanisms of
704 Immune Evasion in Colorectal Cancer. *Cancer Discov* **2018**;8(6):730-49 doi 10.1158/2159-8290.CD-
705 17-1327.
- 706 45. Spranger S, Bao R, Gajewski TF. Melanoma-intrinsic beta-catenin signalling prevents anti-tumour
707 immunity. *Nature* **2015**;523(7559):231-5 doi 10.1038/nature14404.
- 708 46. Dow LE, Premsrirut PK, Zuber J, Fellmann C, McJunkin K, Miething C, *et al.* A pipeline for the
709 generation of shRNA transgenic mice. *Nat Protoc* **2012**;7(2):374-93 doi 10.1038/nprot.2011.446.
- 710 47. Schatoff EM, Paz Zafra M, Dow LE. Base editing the mammalian genome. *Methods* **2019** doi
711 10.1016/j.ymeth.2019.02.022.
- 712 48. Fellmann C, Zuber J, McJunkin K, Chang K, Malone CD, Dickins RA, *et al.* Functional identification
713 of optimized RNAi triggers using a massively parallel sensor assay. *Mol Cell* **2011**;41(6):733-46.
- 714 49. O'Rourke KP, Ackerman S, Dow LE, Lowe SW. Isolation, Culture, and Maintenance of Mouse
715 Intestinal Stem Cells. *Bio Protoc* **2016**;6(4).
- 716 50. O'Rourke KP, Dow LE, Lowe SW. Immunofluorescent Staining of Mouse Intestinal Stem Cells. *Bio*
717 *Protoc* **2016**;6(4).
- 718 51. Dobin A, Davis CA, Schlesinger F, Drenkow J, Zaleski C, Jha S, *et al.* STAR: ultrafast universal RNA-
719 seq aligner. *Bioinformatics* **2013**;29(1):15-21 doi 10.1093/bioinformatics/bts635.
- 720 52. Bray NL, Pimentel H, Melsted P, Pachter L. Near-optimal probabilistic RNA-seq quantification. *Nat*
721 *Biotechnol* **2016**;34(5):525-7 doi 10.1038/nbt.3519.
- 722 53. Love MI, Huber W, Anders S. Moderated estimation of fold change and dispersion for RNA-seq data
723 with DESeq2. *Genome Biol* **2014**;15(12):550 doi 10.1186/s13059-014-0550-8.
- 724 54. Garrido-Martin D, Palumbo E, Guigo R, Breschi A. ggsashimi: Sashimi plot revised for browser- and
725 annotation-independent splicing visualization. *PLoS Comput Biol* **2018**;14(8):e1006360 doi
726 10.1371/journal.pcbi.1006360.
- 727
- 728

729 **Figure Legends**

730 **Figure 1. Tankyrase inhibition drives differentiation in Apc-silenced intestinal tumors.**

731 **a.** Schematic depiction of the animal models and treatments to produce adenomas in vivo. For consistency,
732 Apc^{Min} mice were administered dox at 8 weeks (when tumors are first detectable), and continued for 8-12
733 weeks. shApc and Apc^{Min} mice were treated with G007-LK (30mg/kg) or vehicle for 1 week, then sacrificed to
734 assess tumor burden. **b.** Immunohistochemical, immunofluorescent, and in situ hybridization (Lgr5) stains of
735 representative small intestinal adenomas from shApc mice as indicated. Adjacent normal crypt-villus
736 architecture and shApc off dox (1 week) are shown for reference. **c.** Quantitation of the fraction of BrdU
737 positive cells in individual tumors (n=3-6 tumors/mouse, n=3-6 mice/treatment). Bars show the mean and 95%
738 CI. **d.** Immunohistochemical, immunofluorescent, and in situ hybridization (Lgr5) stains of representative small
739 intestinal adenomas from Apc^{Min} mice as indicated. **e.** Immunofluorescent images of shApc and Apc^{Min}
740 organoids cultured in DMSO or G007-LK (1 μ M) for 3 days. Organoids were pulsed with EdU for 4 hours to
741 label proliferative cells. **f.** Quantitative RT-PCR analysis of gene expression of stem cell (Lgr5) and
742 differentiation (Krt20) markers in shApc and Apc^{Min} organoids cultured in DMSO or G007-LK (1 μ M) for 3
743 days (n=3, error bars = s.e.m., * p-value < 0.05, unpaired t-test with Welch's correction).

744

745 **Figure 2. Sustained Tnks1/2 knockdown is sufficient to block shApc-mediated tumorigenesis.**

746 **a.** Schematic of the experimental strategy to achieve Tnks1/2 knockdown in shApc and Apc^{Min} adenomas. **b.**
747 Colonic endoscopy images taken 4 and 8 weeks post 4-OHT/dox treatment in shApc or shApc//shTnks1/2 mice
748 show a dramatic difference in adenoma formation. **c.** Epifluorescent images of whole mount colon from shRen,
749 shApc, shApc//shTnks1/2, Apc^{Min}//shRen, and Apc^{Min}//shTnks1/2 mice sacrificed at the experimental
750 endpoint; Black signal represents GFP fluorescence. Immunohistochemical (H&E) and immunofluorescent
751 (BrdU/Keratin20) stains of representative small intestinal adenomas from mice sacrificed at experimental
752 endpoint. **d.** Quantitation of tumor burden from H&E stained sections of each genotype, as indicated. Tumor
753 area was calculated as a percentage of total tissue in representative cross-sections of the small intestine and
754 colon (n=4-5, error bars = s.e.m., ** p-value < 0.005, unpaired t-test with Welch's correction). **e.** Kaplan-Meier
755 plot showing survival of each genotype, as indicated. Log-rank statistical tests are available in [Table S5](#). **f.**
756 Hematocrit from peripheral blood of each genotype at experimental endpoint (n=3-8, error bars = s.e.m., * p-
757 value < 0.05, unpaired t-test with Welch's correction).

758

759 **Figure 3. An MCR truncation in Apc sensitizes organoids to Tnks1/2 blockade**

760 **a.** Lollipop plot of publicly available human CRC MSK-IMPACT and PanCan data showing mutation frequency
761 across all codons in APC. **b.** Scatter plot of MSK-IMPACT and PanCan data from CRCs carrying two distinct
762 mutations in APC, highlights the presence of late truncating mutations in most CRCs. **c.** Apc mutations
763 generated in organoids. **d.** Brightfield images of Apc-mutant or β cat^{S33F} organoids treated with DMSO or G007-

764 LK (1 μ M) as indicated. **e.** Quantitation of viable organoids after 7 days of DMSO or G007-LK treatment (n=3-
765 4, error bars = s.e.m., * p <0.05, unpaired t-test with Welch's correction). All organoids were passaged once at
766 day 3. **f.** Heatmap representing relative gene expression in wildtype, Apc and β cat^{S33F} organoids cultured in
767 DMSO or G007-LK for 3 days. Shown are 1472 genes with a log₂FC >2 and adj. p-value <0.01 in G007-LK-
768 treated WT organoids, compared to DMSO controls. **g.** Summary plot of GSEA results, including 10
769 significantly positively and negatively enriched gene sets in G007-LK treated Apc^{Q1405X} organoids. Leading
770 Edge Fraction (LEF) is the fraction of genes in the geneset included in the leading edge of the GSEA plot. **h.**
771 Mean expression of 18 validated WNT target genes (Table S2) following 3 days treatment with G007-LK or
772 DMSO, normalized to DMSO-treated WT organoids. **i.** Schematic depiction of the cell populations identified by
773 gene signatures in Kim et al. 2014. Adjacent color-coded volcano plots of G007-LK treated Apc^{Q1405X} and
774 Apc^{Q884X} organoids highlight genes included in these signatures. Genes upregulated following G007-LK
775 treatment are shifted to the right. **j.** Immunofluorescent staining of Apc-mutant or β cat^{S33F} mutant organoids
776 cultured in DMSO or G007-LK (1 μ M) for 3 days. Organoids were pulsed with EdU for 4 hours to label
777 proliferative cells.

778
779 **Figure 4. Human cells and ApcQ1405X mouse adenomas with MCR truncations respond to Tnks1/2**
780 **inhibition.**

781 **a.** Western blot of DLD1 cells expressing Cas9, transduced with sgRNAs targeting either FANCF1 (negative
782 control) or APC (near codon Q884). Targeting with the APC sgRNA generated a shorter truncated protein. **b.**
783 Expression of WNT target genes *LGR5* and *AXIN2* in FANCF1 or APC^{Q884} transduced DLD1s following 72
784 hrs. treatment with G007-LK, as indicated. **c.** Expression of WNT target genes *LGR5* and *AXIN2* in patient-
785 derived organoids following 72 hrs. treatment with G007-LK, as indicated. Raw values of individual replicate
786 experiments are presented in Supplementary Figure 11. **d.** Immunoprecipitation of Axin1 in whole cell lysates
787 from Apc^{Q1405X} and Apc^{Q884X} cells treated with G007-LK or DMSO for 24 hours. **e.** Kaplan-Meier plot showing
788 survival of Apc^{Q1405X} mice (red line) as compared to Apc^{Min} mice (blue line). **f.** Bar graph showing hematocrit
789 from Apc^{Q1405X/+} and Apc^{+/+} mice at 10-11 weeks. **g.** Immunohistochemical, immunofluorescent, and in situ
790 hybridization (*Lgr5*) stains from the proximal small intestine of 10-week-old Apc^{Q1405X} mice treated with vehicle
791 or G007-LK (30mg/kg, QD) for one week. Apc^{Q1405X} mice treated with G007-LK show a differentiation profile
792 marked by decreased BrdU incorporation, decreased *Lgr5* abundance, and increased alkaline phosphatase
793 staining. **h.** Quantitation of the fraction of BrdU positive cells (left) and Alkaline phosphatase positive area
794 (right) in individual tumors (n=3-6 tumors/mouse, n=3-6 mice/treatment). Bars represent mean and 95% CI. **i.**
795 Model for data presented, indicating that late truncating mutations in Apc, but not early truncating mutations can
796 engage the destruction complex in response to Tnks1/2 inhibition. Subsequent DC assembly re-establishes
797 normal control of WNT signaling. DC assembly re-establishes normal control of WNT signaling.

Figure 1

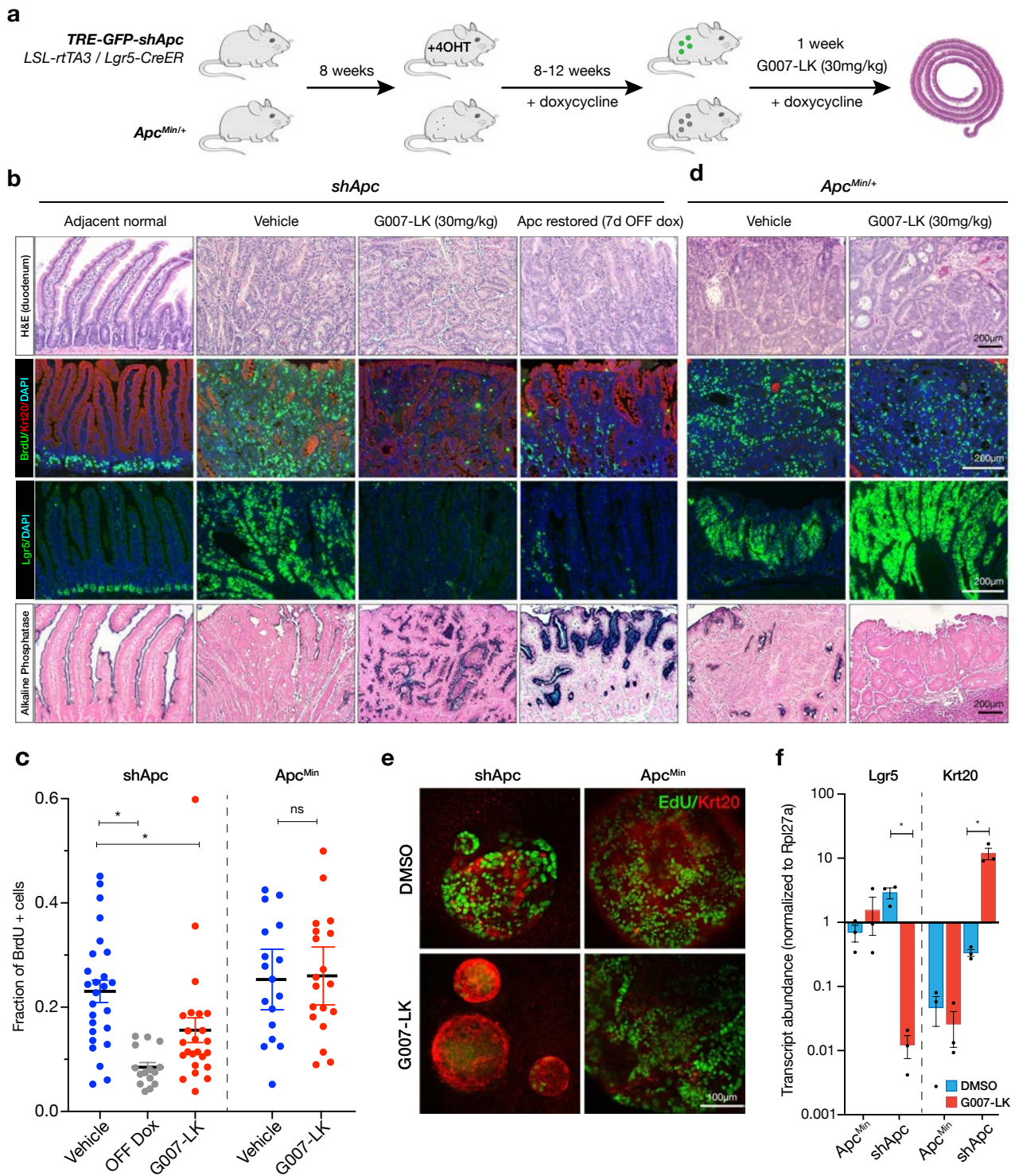
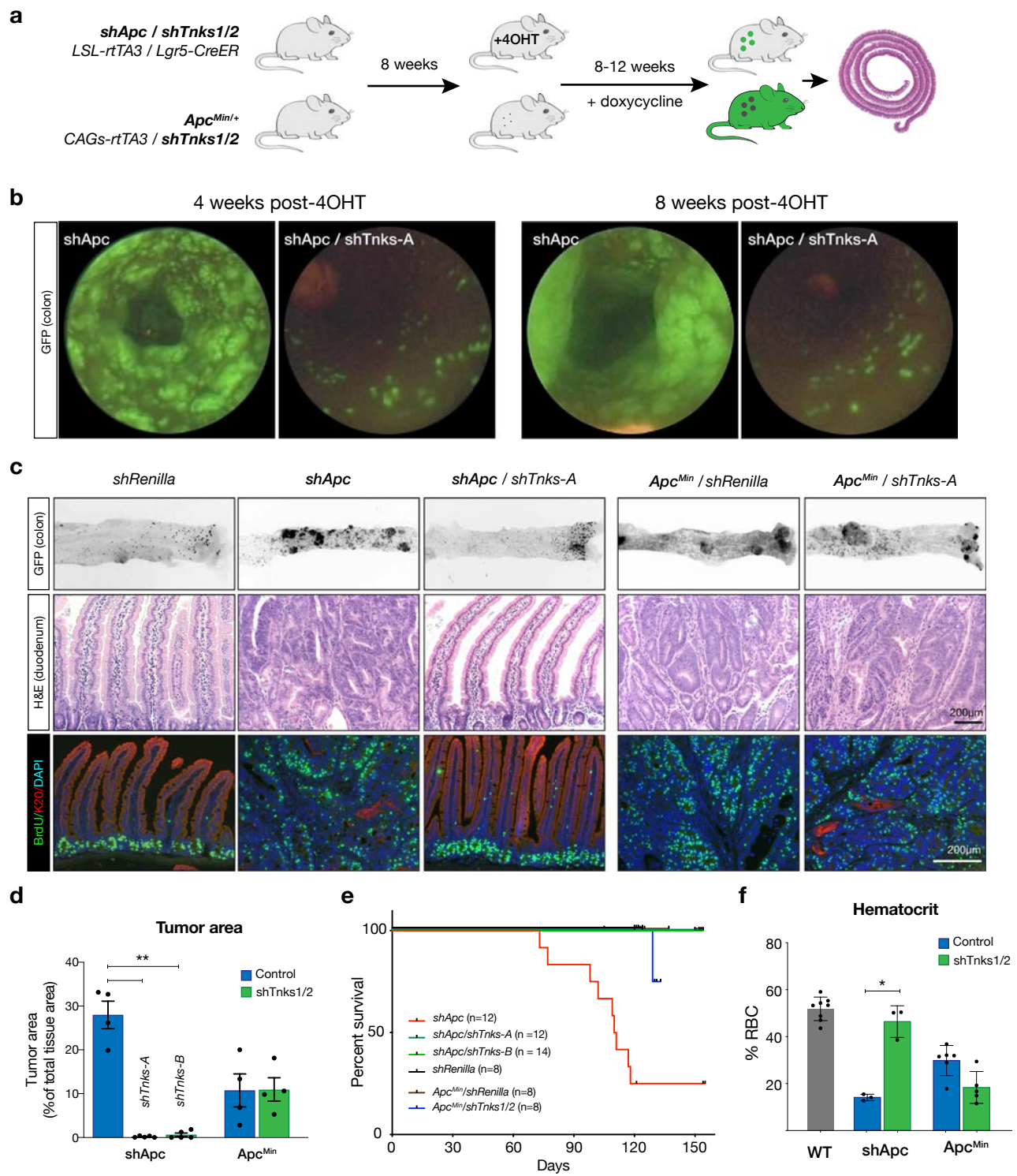


Figure 2



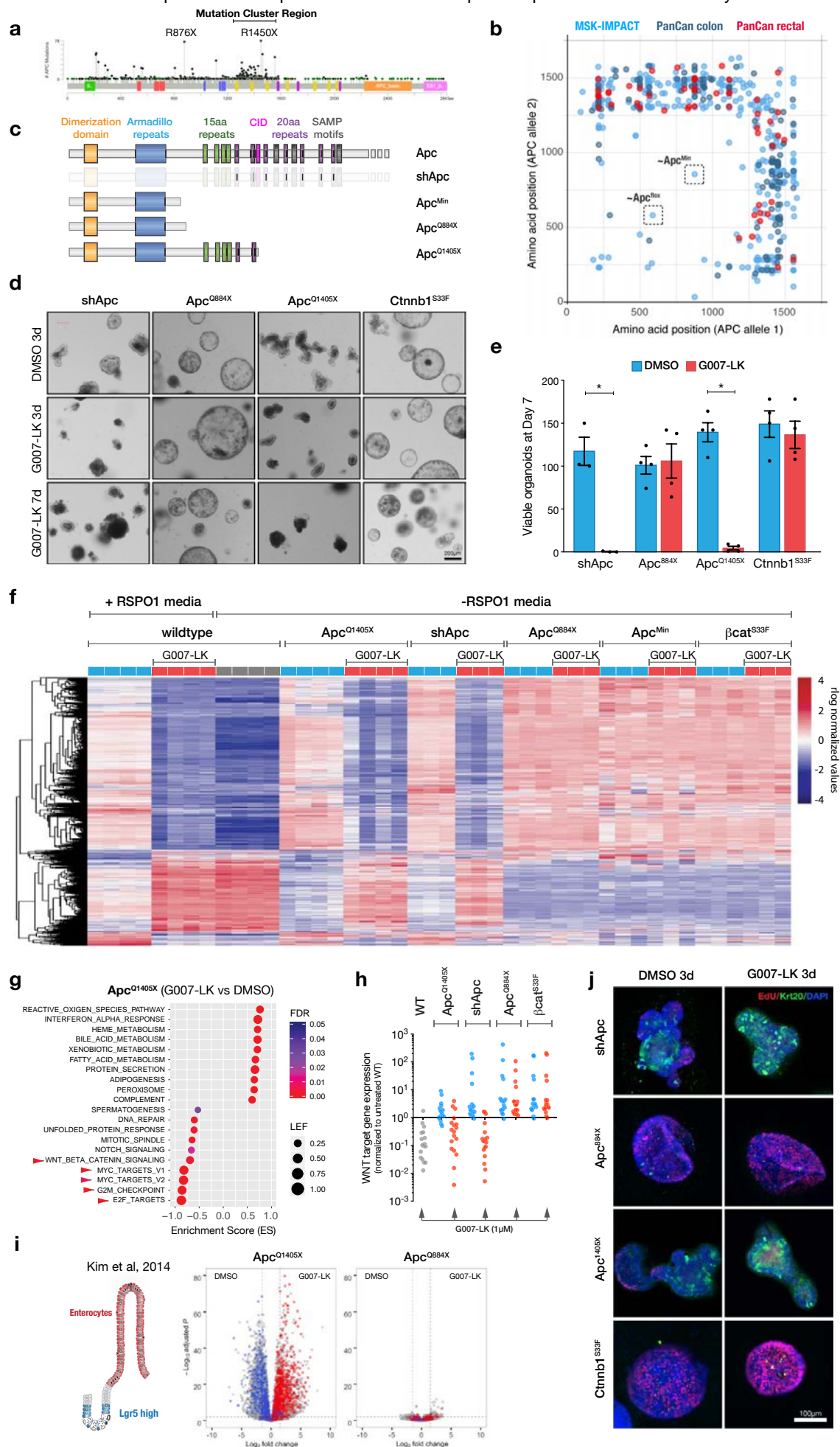
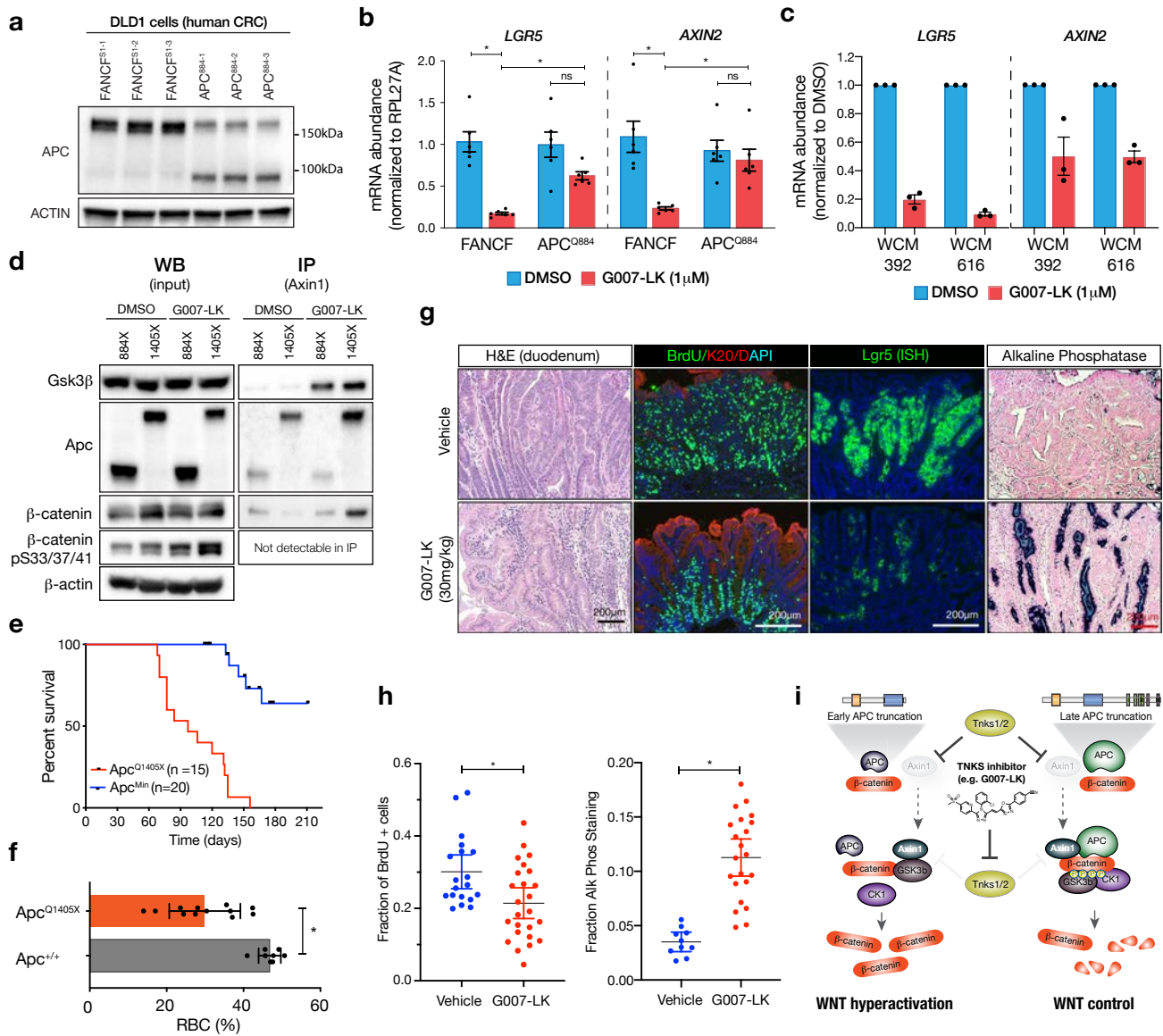


Figure 4



CANCER DISCOVERY

Distinct CRC-associated APC mutations dictate response to Tankyrase inhibition

Emma M Schatoff, Sukanya Goswami, Maria Paz Zafra, et al.

Cancer Discov Published OnlineFirst July 23, 2019.

Updated version	Access the most recent version of this article at: doi: 10.1158/2159-8290.CD-19-0289
Supplementary Material	Access the most recent supplemental material at: http://cancerdiscovery.aacrjournals.org/content/suppl/2019/07/23/2159-8290.CD-19-0289.DC1
Author Manuscript	Author manuscripts have been peer reviewed and accepted for publication but have not yet been edited.

E-mail alerts [Sign up to receive free email-alerts](#) related to this article or journal.

Reprints and Subscriptions To order reprints of this article or to subscribe to the journal, contact the AACR Publications Department at pubs@aacr.org.

Permissions To request permission to re-use all or part of this article, use this link <http://cancerdiscovery.aacrjournals.org/content/early/2019/07/23/2159-8290.CD-19-0289>. Click on "Request Permissions" which will take you to the Copyright Clearance Center's (CCC) Rightslink site.